Volume 22
Number 13
7 July 2022
Pages 2395–2592

Lab on a Chip

Devices and applications at the micro- and nanoscale

rsc.li/loc

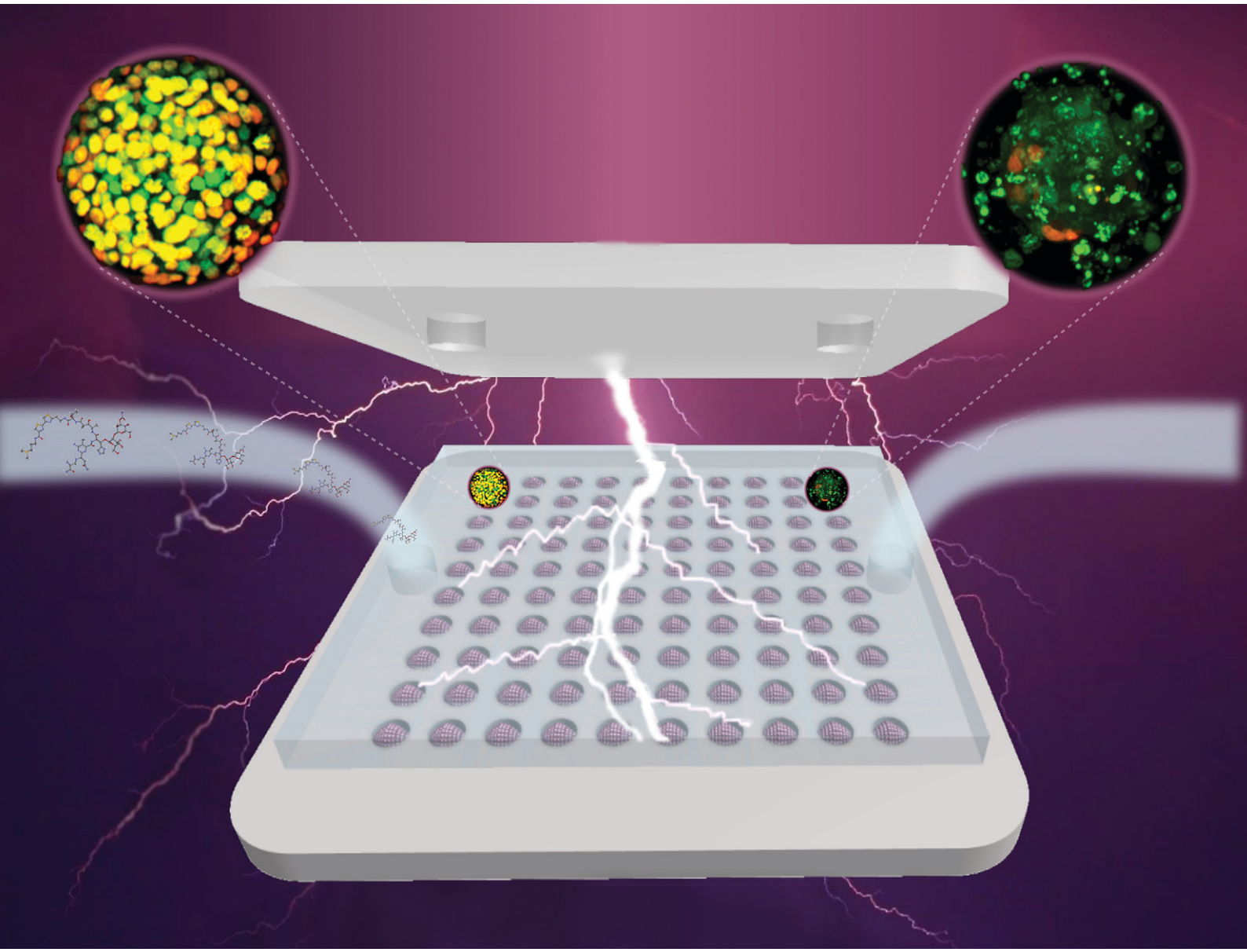

ISSN 1473-0197

ROYAL SOCIETY OF CHEMISTRY

PAPER

Pauline Bregigeon, Marie Frénéa-Robin *et al.*
Integrated platform for culture, observation, and parallelized electroporation of spheroids

Lab on a Chip

PAPER

View Article Online
View Journal | View Issue

Cite this: *Lab Chip*, 2022, **22**, 2489

Integrated platform for culture, observation, and parallelized electroporation of spheroids†

Pauline Bregigeon, *[a] Charlotte Rivière, [bcd] Laure Franqueville,[a] Christian Vollaire,[a] Julien Marchalot [a] and Marie Frénéa-Robin *[a]

Reversible electroporation is a method to introduce molecules into cells by increasing the permeability of their membranes, thanks to the application of pulsed electric fields. One of its main biomedical applications is electro-chemotherapy, where electroporation is used to deliver anticancer drugs into tumor tissues. To improve our understanding of the electroporation effect on tissues and select efficient treatments, *in vitro* tumor models are needed. Cell spheroids are relevant models as they can reproduce tumor microenvironment and cell–cell interactions better than 2D cell cultures. Various methods offering a relatively simple workflow are now available for their production. However, electroporation protocols usually require handling steps that may damage spheroids and result in random spacing, inducing variations in electric field distribution around spheroids and non-reproducible electroporation conditions. In addition, only a few microsystems allow the production and electroporation of spheroids, and the spheroids produced lack reproducibility in size and location. To overcome these issues, we developed a unique device enabling culture, monitoring, and electroporation of hundreds of regular spheroids in parallel, with a design ensuring that all spheroids are submitted to the same electric field conditions. It is comprised of a microfluidic chamber encompassing a micro-structured agarose gel, allowing easy medium exchange while avoiding spheroid handling. It also enables optical imaging of spheroids *in situ*, thanks to transparent electrodes. In this paper, we describe the fabrication and characterization of the developed microsystem and demonstrate its applicability to electroporation of a network of spheroids. We present a first successful application as an anticancer drug testing platform, by evaluating the bleomycin effect on HT29 colorectal cancer cell spheroids. This work opens new perspectives in the development of *in vitro* assays for the preclinical evaluation of electroporation-based treatment.

Received 21st January 2022,
Accepted 15th April 2022

DOI: 10.1039/d2lc00074a

rsc.li/loc

Introduction

Cancer treatment by chemotherapy, usually delivered by systemic routes, is limited due to the toxicity of chemotherapeutic agents and leads to numerous short-term and long-term side effects. In the search for a safer and more efficient treatment, electro-chemotherapy (ECT) has emerged as a solid alternative.[1] This method is based on the combination of local delivery of non-permeant drugs and permeabilization of cell membranes to facilitate the introduction of these drugs into cells. This electro-permeabilization of cells, historically known as reversible electroporation (EPN), is a technique using pulsed electric fields to enhance cell permeability, developed since the 1970s.[2,3] ECT increases the uptake of cytotoxic drugs, up to 1000-fold in the case of bleomycin for instance.[4] This technology is now implanted in more than 150 cancer treatment centers in Europe[5] and is also employed in veterinary oncology around the world, with more than 4000 animals treated with ECT in 2015.[6] EPN also allows efficient delivery of plasmid DNA encoding therapeutic genes into cells and tissues, which is referred to as electro-gene therapy (EGT). Both preclinical and clinical recent studies have indicated a systemic immune response could be induced by a combination of ECT and EGT,[5,7] increasing even more the interest of EPN-based treatments.

Full exploitation of the huge potential of these treatments requires a thorough understanding of the effect of electrical pulses on cells, and therefore the development of reliable *in vitro* models reproducing as accurately as possible the *in vivo* tumor microenvironment. In a first approach, 2D cell cultures and cell suspensions have been used for theoretical

[a] *Univ Lyon, Ecole Centrale de Lyon, INSA Lyon, Université Claude Bernard Lyon 1, CNRS, Ampère, UMR5005, 69130 Ecully, France.*
E-mail: pauline.bregigeon@ec-lyon.fr, marie.robin@univ-lyon1.fr
[b] *Univ Lyon, Université Claude Bernard Lyon 1, CNRS, Institut Lumière Matière, F-69622, Villeurbanne, France*
[c] *Institut Universitaire de France (IUF), France*
[d] *Institut Convergence PLAsCAN, Centre de Cancérologie de Lyon, INSERM U1052-CNRS UMR5286, Université de Lyon, Université Claude Bernard Lyon 1, Centre Léon Bérard, Lyon, France*

† Electronic supplementary information (ESI) available. See DOI: https://doi.org/10.1039/d2lc00074a

and experimental studies.[8,9] However, both these models lack cell–cell interactions and do not reproduce the complexity of the tumor microenvironment, which was shown to be of great importance during carcinogenesis.[10] To overcome these limitations, recent studies have focused on more complex 3D cell models.[10] Among them, spheroids have regained interest in the community.[11,12] Spheroids are 3D cell aggregates able to mimic the organization of a tumor, thanks to nutrients and dioxygen concentration gradients[13] as well as cellular cohesion and communication, allowing for a reliable assessment of new anticancer treatment efficacy.[14] Indeed, by monitoring spheroid growth and by performing biochemical analysis (*e.g.* cell proliferation inside the spheroids), it is possible to determine the adequate electric field parameters for efficient EPN and to evaluate the efficiency of potential anticancer drug.[15] Therefore, spheroids enable a more reliable prediction of the EPN effect compared to 2D *in vitro* models. They can be produced with human cells, and as such appear like a good preclinical model ahead of *in vivo* experiments.[16] Several methods of spheroid production have been developed in the last decades.[10] One of the most commonly used is the hanging-drop method, where cells aggregate at the tip of a drop to form one spheroid. A large number of spheroids of similar size can be produced with this technique thanks to hanging-drop plates,[17] but changing the medium in these plates can disturb spheroid growth. Another method quite used is based on ultra-low attachment 96-well plates, allowing the spontaneous formation of spheroids, but with a heterogeneous size distribution.[10] This might potentially affect the reproducibility, as it has been shown that spheroid size can influence their sensibility to pulsed electric field.[18] Other methods of spheroid production based on the use of agarose microwells integrated in a microfluidic chip have been developed more recently, for drug screening application.[19,20] However, they do not allow the application of a pulsed electric field.

To perform EPN on the spheroids, a commonly used approach is to introduce them in solution in a cuvette containing two parallel metal electrodes, typically separated by a few millimeters, connected to a commercial electroporator.[21,22] This approach requires experimental steps that may damage spheroids (centrifugation or agitation). Furthermore, it may lead to the random distribution of spheroids inside the cuvette, thereby inducing differences in the electric field perceived from one spheroid to the other. Alternatively, hand-held electrodes connected to electroporators were developed to apply pulsed electric field around spheroids cultivated in 96-well plates.[15,23] However, spheroids are treated one by one, which can be laborious and time-consuming. To overcome these issues, microfluidic-based devices integrating the possibility to perform EPN on the produced spheroids have been developed.[24] They provide several advantages such as reduction of inter-electrode distance (and therefore of the applied voltage), better control of electric field distribution with respect to cell position, lower risk of sample contamination, limitation of cell manipulation, and integration of more functionality with reduced footprint and improved portability.[25] However, there are few existing microsystems allying microfluidics and electronics to perform EPN on 3D cell assemblies,[26,27] and their use might be limited by complex micro-electrode design.[28] In addition, microsystems allowing EPN of 3D cell spheroids do not currently enable the parallel production of many spheroids with regular characteristics[29] and deterministic positioning.

Based on this statement, we developed a microfluidic system combining the production of spheroids of controlled and reproducible size, shape, and spacing on one hand, and EPN with simple transparent electrodes allowing uniform electric field distribution and *in situ* monitoring with optical techniques on the other hand. This device aims to simplify electroporation procedures on spheroids by providing easiness of use, simultaneous treatment of a large number of spheroids, and reproducibility of the results. The approach is based on the use of a molded agarose hydrogel containing hundreds of microwells enabling the production of a network of spheroids of uniform size and regularly spaced.[30,31] The developed system allows rapid medium exchange before application of EPN pulses, without disturbing the spheroids while avoiding the stress induced by centrifugation or washing steps usually required for EPN. Furthermore, its integration in a dedicated electrical system allows circumventing one of the limitations of commercial electroporators, that do not allow the use of sine bursts. The interest of such waveforms has been recently demonstrated, as they enable to reduce electrode fouling[32] and to perform frequency analysis of cell response to electrical stimuli.[33]

In this work, we fully characterized the designed microsystem and conducted a proof-of-concept study validating its functionality as a platform for production, monitoring, and reversible electroporation of numerous spheroids in parallel, thanks to the calibration of electric field parameters. We demonstrated that the microsystem enables direct monitoring of spheroids with several optical techniques, including confocal microscopy, during their formation and following EPN treatments. It allowed to characterize EPN efficiency in the core of spheroids and to perform bio-analysis easily, such as proliferation labelling test. We further developed a first assay for *in vitro* evaluation of ECT treatment, by testing the efficiency of bleomycin combined with EPN on HT29 colorectal cancer cell spheroids.

Experimental

Design and fabrication of the EPN device

The device is composed of a microfluidic chamber made of two conductive glass slides containing an agarose hydrogel microwell array.[34] A micromachined sealing device made of poly(methyl methacrylate) (PMMA or Plexiglas®) ensures liquid medium tightness and enables electrical contact (Fig. 1).

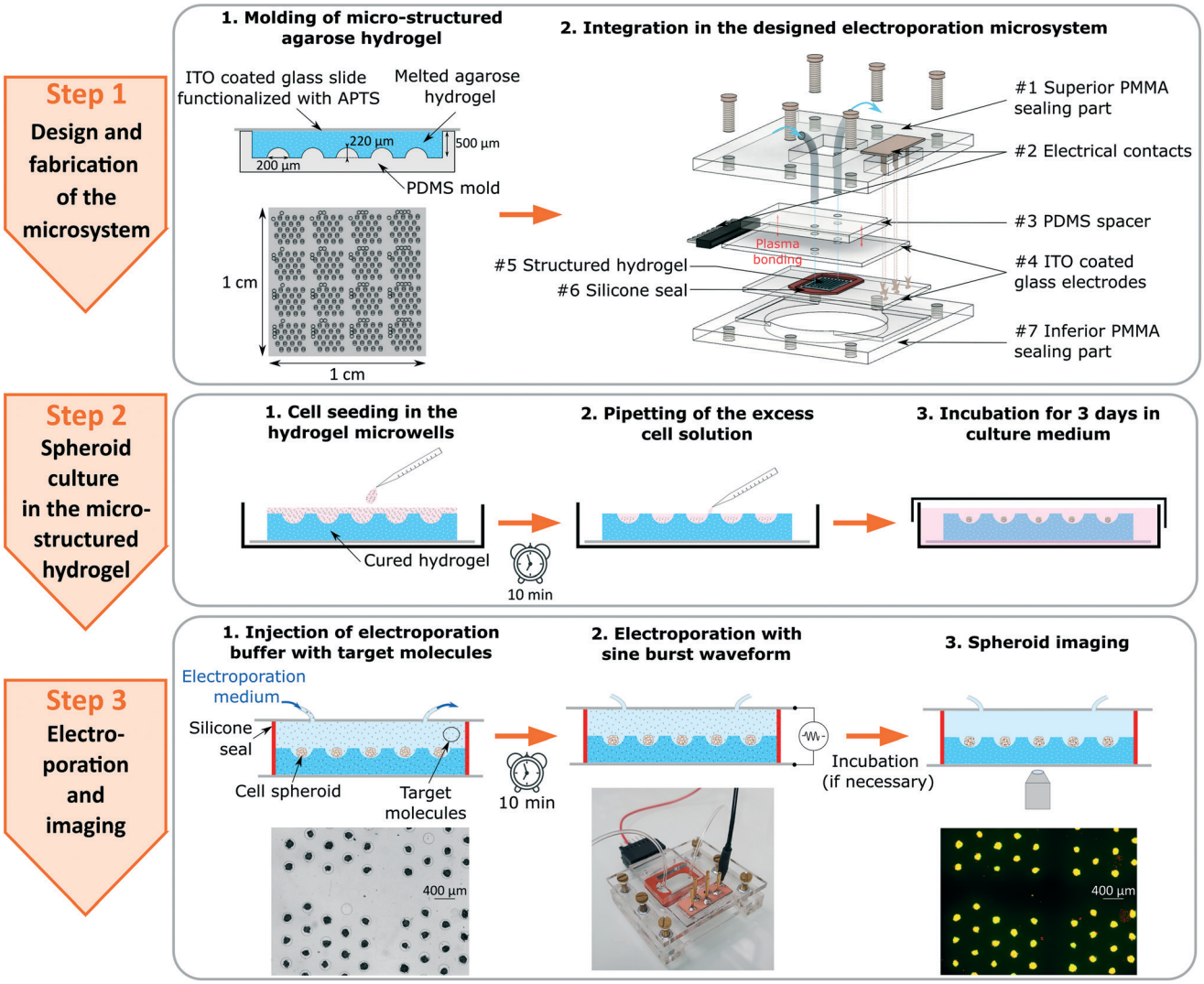

Fig. 1 Design, fabrication and use of the microsystem as culture and electroporation platform. (Step 1) Fabrication of the device: schematic drawing of the molding process and the microwell array obtained (1.1), exploded view of the device (1.2). (Step 2, 2.1 to 2.3) Protocol of spheroid culture in the micro-structured hydrogel. (Step 3) Electroporation and imaging: injection of the EPN buffer in the device containing grown HT29 cell spheroids (2.5× bright field image, 3.1), subsequent electroporation in the mounted device (picture, 3.2), and imaging with confocal or epifluorescence microscopy (2.5× green and red merged epifluorescence image after EPN of HT29 cell spheroids in presence of FDA and PI, 3.3).

A micro-milled metal master mold was first created using 200 µm micro-mill (Dixi Polytool 7032, diameter 200 µm, length 300 µm) to create an array of 320 semi-spherical microwells of 200 µm diameter, 220 µm depth (Fig. SI 1†). A reusable polydimethylsiloxane (PDMS) mold was then made from this master mold with a replica molding process. A 2% (w/v) agarose solution was prepared by dissolving standard agarose (Merck) in deionized water. The solution was autoclaved and kept at 78 °C. A thin layer of this solution (100 µL) was poured onto the pre-warmed PDMS mold and a pre-warmed indium tin-oxide (ITO) coated glass slide (Merck) was placed over it before gelation and demolding (Fig. 1, step 1.1). This slide had first been functionalized with (3-aminopropyl)triethoxysilane (APTS) (Merck) solution (1% APTS and 5 mM acetic acid in deionized water) so that the hydrogel could bond to it.[30] The glass slide covered with the micro-structured hydrogel was placed in a Petri dish with phosphate-buffered saline without calcium and magnesium (PBS w/o Ca Mg, Dutscher) and sterilized with UV light for 25 min (24 W, 254 nm).

To mount the device (Fig. 1, step 1.2), a 1 mm-high silicone seal (part #6, Grace Bio-Labs, Merck), cut to size using a Silhouette Cameo cutting machine, was placed around the hydrogel (part #5) to form the microfluidic chamber, which was closed on top with another ITO coated glass slide (part #4). The spheroid-containing hydrogel was thereby sandwiched between two conductive glass slides used as electrodes for EPN. Two holes were drilled in the top slide using micro-abrasive blasting (Microblaster®, Comco Inc). A PDMS slab (part #3) in which holes were also punched was aligned and bonded to it with air plasma (using a Harrick plasma cleaner), thereby enabling to fix connecting tubes for

medium injection. Two plexiglass pieces (part #1 and #7) micromachined with a laser cutter (Speedy 400, Trotec) were screwed to seal the device. They were also designed to enable interfacing with electrical equipment (part #2). The transparency of plexiglass allows for easy mounting (checking the apparition of bubbles in the microfluidic chamber for example) and the hole on the inferior sealing part enables *in situ* imaging of spheroids with an inverted microscope (Fig. 1, step 3.3).

Cell culture in the hydrogel scaffold

HT29 colorectal cancer cells, obtained from American Type Culture Collection (ATCC, USA) were cultured in high glucose Dulbecco's modified Eagle's medium (DMEM, Dutscher) supplemented with 10% of heat-inactivated fetal bovine serum (FBS, Dutscher), 1% of MEM non-essential amino acids 100× (NEAA, Dutscher) and 1% of penicillin/streptomycin 100× (Dutscher). Cells were grown in T-25 cell culture flasks in an incubator at 37 °C with a humidified 5% CO_2 atmosphere and routinely sub-cultured every 3 days. To seed the hydrogel micro-wells, cell passage was realized with trypsin EDTA 10× (Dutscher) to detach cells. They were resuspended in culture medium, counted with Neubauer chamber, and centrifugated at 1200 rpm for 3 min. A determined volume of culture medium was added to the cell pellet to reach the desired cell concentration.

A volume of 200 μL of the homogenized cell suspension solution containing 50 000 cells was added on top of the micro-structured hydrogel, placed in a 60 mm Petri dish. The cells were left to sediment in the bottom of the microwells for 10 min. The excess cells were then removed by pipetting the excess solution, and 5 mL of culture medium were added (Fig. 1 step 2). Seeded hydrogels were incubated for 3 days to form an array of spheroids of controlled and uniform characteristics (size and position), as demonstrated in Fig. SI 2.† The number of cells sedimented in each well was estimated by comparing spheroid size at 3 days of culture obtained with this method, with the one obtained with the classic ultra-low adhesion (ULA) 96-well plates. Approximately 30–40 cells sediment in each microwell during the seeding.

Operation procedure for spheroid electroporation

To perform electroporation on the grown spheroids, the culture medium was removed and the slide with the micro-structured hydrogel was mounted in the microsystem as previously described, after having cleaned all parts with 70% ethanol. The EPN buffer had a low conductivity of 0.03 S m^{-1}, to minimize undesirable effects such as electrolytic reactions or heating by Joule effect.[33] It was composed of 10 mM of Hepes (Merck), 1 mM of magnesium chloride hexahydrate ($MgCl_2$ ($6H_2O$), Merck) and 250 mM of saccharose (Roth) dissolved in deionized water, with a few drops of 10 M sodium hydroxide (NaOH, Merck) to adjust pH to 7.1. The injection of EPN buffer (Fig. 1, step 3.1), supplemented with appropriate target molecules, was realized with a calibrated time and volume for complete medium exchange (see section "Medium exchange inside the hydrogel").

The microsystem was then connected to the electroporation system (Fig. 1, step 3.2), composed of an arbitrary waveform generator (3310A, Agilent Technologies) to apply the pulsed electric field, amplified by a high-speed bipolar amplifier (HAS 4051, NF Corp). An oscilloscope (DSO5012A, Agilent Technologies) was also used to monitor the input voltage and the output current, the latter being measured with a current sensor (HY 5-P, LEM). The pulse parameters used for EPN were determined as explained in the next sections. Imaging of spheroids was usually performed *in situ*.

For long-term follow-up, the device was carefully disassembled and the slide containing spheroids was put back in the initial Petri dish with culture medium. Spheroid growth could then be followed for several days.

Estimation of voltage drop and electric field distribution

The electrical potential effectively applied on the electrode was determined by estimating the voltage drop due to electrical contacts and wires from impedance measurements made with a precision impedance analyzer (4294A, Agilent Technologies) in the device containing EPN buffer. The measured impedance was fitted to a theoretical model detailed in Fig. SI 3.†

To evaluate the effective electric field perceived by spheroids, electric field distribution in the microfluidic chamber was also determined, thanks to COMSOL modelling. The module "Electric Currents in Layered Shells" allowed to model the ITO conductive layer of the electrodes. Its conductivity (7×10^5 S m^{-1}) was measured with a 4-points measurement technique and its thickness (134 ± 4 nm) was measured with profilometry technique. Those layers sandwiched a block representing the microfluidic chamber filled with EPN medium in absence of cells. The potential applied to the terminals of the electrodes in the simulation was the rms value of the highest potential tested in the experiments.

Medium exchange inside the microfluidic chamber

To characterize medium exchange inside the microfluidic chamber containing the hydrogel, impedance measurements were realized with a precision impedance analyzer. The hydrogel, without spheroids, was first incubated 24 h in culture medium. It was then mounted in the device and EPN buffer was injected with a 2.5 mL syringe and 21G needle by 0.5 mL every 1.5 min. Impedance measurements were made after each injection to monitor the evolution of overall conductivity inside the chamber, reflecting ions and molecules diffusion for the hydrogel part of the chamber. To confirm these results, another experiment was made with optical technique (confocal microscopy) to monitor the diffusion of a fluorescence solution (0.05 mM FITC in PBS) inside the hydrogel (Fig. SI 4†).

Determination of EPN parameters and evaluation of EPN efficiency

EPN tests were then performed on the fully characterized device, to calibrate the parameters and evaluate EPN efficiency. The excitation pulses used in this study were sine bursts. The optimal frequency was chosen to minimize the voltage drop in the microsystem and to maximize the effect of the pulsed electric field on HT29 cells. This was determined by predicting the effective voltage in the electrolyte accounting for double layer effects and voltage drop due to contacts and wires, and characterization of the evolution of transmembrane potential (TMP) for HT29 cells (Fig. SI 3†). Two sine bursts of 10 kHz frequency and 5 ms duration, spaced by 1 s, were applied.[33] Several amplitudes of sine burst were tested to determine the efficient EPN parameters. Values from 100 to 300 V_{pp} (peak-to-peak) were tested to sweep a range of equivalent effective electric fields of 300 to 900 V_{RMS} cm^{-1} inside the chamber containing the spheroids.

To determine the EPN efficiency and to assess the viability of cells, two fluorophores were used: fluorescein di-acetate (FDA, Merck) to label living cells in green, and propidium iodide (PI, Merck), to label dead or electroporated cells in red (explanations detailed in Fig. SI 5†). PI and FDA were added to the EPN buffer, with respective proportions of 30 μM and 12 μM, before injection inside the microfluidic chamber.

The pulsed electric field was then applied with the chosen parameters (2 sine bursts, 10 kHz, 5 ms, 100 to 200 V_{pp}). Cell spheroids were observed 5 min after EPN with an epifluorescence microscope (AxioImager M1, Zeiss) on 5 focus planes of the spheroids. A maximum intensity projection (MIP) was realized with the ImageJ software and the mean red fluorescence intensity was evaluated for about 12 spheroids per tested condition.

Additionally, to evaluate cell mortality depending on the applied EPN voltage, cell spheroids were electroporated at 200 or 300 V_{pp} in EPN buffer, then incubated 2 h in cell culture medium and labelled with FDA and PI in PBS for observation with confocal microscopy (Leica SP5, Fig. SI 6†).

To further characterize electroporation efficiency inside cell spheroids, and test higher voltages, observations with a confocal 25× water immersion objective (NA 0.95) were realized on fixed samples. Cell spheroids were electroporated (2 sine bursts, 10 kHz, 5 ms, 100 to 300 V_{pp}) in the designed microsystem with EPN buffer containing PI and FDA (respectively 30 and 12 μM) and incubated 15 min in cell culture medium. They were then fixed with 4% paraformaldehyde (PFA, Merck) in PBS for 20 min, with three PBS rinses before and after fixation. A negative control with dead spheroids, incubated 30 min in 70% ethanol, was also studied. To overcome the limitations of optical sectioning techniques like confocal microscopy, a clarification of spheroids was performed to uniformize the refractive indexes in the samples. To do so, 8 : 20 glycerol in PBS solution was used as previously described.[31,35] Confocal microscopy enabled the acquisition of images in the *z*-direction with a 2 μm *z*-step. Images were analyzed with a Matlab routine already described.[31] Briefly, the spheroids were segmented at each *z* position thanks to the PI red fluorescence and each slice of spheroids was fitted into a perfect circle. In the perfect sphere obtained by combining all *z* slices, coordinates were changed from cartesian to spherical to evaluate the mean red fluorescence intensity from spheroids periphery to core, therefore assessing the EPN efficiency inside spheroids for different applied voltages. The maximum red fluorescence intensity on the whole spheroid could also be determined, allowing to compare fluorescence levels between dead and electroporated cells.

Application to electro-chemotherapy with bleomycin: growth monitoring and proliferation assay

A first application of the device to *in vitro* study of electro-chemotherapy treatment on 3D cell constructs was realized in the developed microsystem with bleomycin, a non-permeant anticancer drug only penetrating into cells upon the action of permeabilization of the electric field.[36] A bleomycin (Merck) concentration of 20 μg mL^{-1} (corresponding to 14 μM) was added to the EPN buffer before its injection into the device. The EPN was then realized with the parameters previously described (2 sine bursts, 10 kHz, 5 ms, 200 V_{pp}). Bleomycin effect on electroporated spheroids was compared to three control groups: spheroids in presence of bleomycin without EPN, spheroids electroporated with EPN buffer only, and spheroids cultured without EPN and bleomycin. Spheroid growth was studied for 3 days after EPN by optical microscope imaging and measuring spheroid diameter thanks to ImageJ software. The ratio of diameter at different time points over diameter before EPN was calculated to compare spheroid growth of the different groups.

To evaluate cell proliferation 3 days after EPN, a proliferation labelling kit (Click-iT EdU Alexa546 Imaging Kit, Invitrogen) was used as indicated by the supplier. EdU (5-ethynyl-2′-deoxyuridine) is a thymidine analog that is incorporated into DNA during active DNA synthesis. After 24 h incubation of spheroids with 10 μM of EdU[37] in culture medium, spheroids were rinsed in PBS, fixed with 4% PFA (20 min), and rinsed with PBS supplemented with 3% of bovine serum albumin (BSA, Promega), to saturate nonspecific sites (3 × 5 min). They were then permeabilized with a Triton X-100 solution (Merck, 0.5% in PBS), and further rinsed with a PBS solution with 3% BSA (3 × 5 min). EdU detection was realized by a specific click reaction between alkyne contained in EdU and azide contained in Alexa Fluor® dye. Spheroids were incubated overnight at 4 °C with NucGreen™ – dead 488 (Invitrogen, 1 drop in 5 mL of PBS) to label cell nuclei. Spheroids were then clarified in a glycerol/PBS solution (80/20 v/v) and observed with a confocal microscope as previously explained. Green fluorescence corresponds to cell nuclei (NucGreen) and red fluorescence

corresponded to proliferative cells (EdU detection). To quantify proliferative cell layer inside the spheroids, the Pearson correlation coefficient, evaluating the colocalization of red and green pixels, was determined with a Matlab routine (Fig. SI 7†).

Statistics

The *p*-values calculated correspond to the two-sample Student *t*-test, allowing to test the hypothesis that two statistical series come from normal distribution with equal means, at a threshold of 5%. Therefore, when this hypothesis is rejected, it cannot be concluded that the two statistical series have the same means, with a precision of 95%. Normal distribution of the series was checked with one-sample Kolmogorov–Smirnov test and variances were calculated to adjust the hypothesis of the Student *t*-test. The tests were performed with Matlab software.

Results and discussion

Design and working principle of the microsystem developed

The design and working principle of the microsystem are presented in Fig. 1. It is composed of a microfluidic chamber made of two transparent parallel electrodes, integrated with sealing parts allowing water tightness, electrical contact, and observation with inverted microscope. This microsystem enables the parallel electroporation of the hundreds of spheroids of similar shape, size, and location that are produced and cultivated in a micro-structured hydrogel bonded on the bottom electrode of the microfluidic chamber. This hydrogel presents several advantages and is widely used in tissue engineering and microfluidic cell culture systems.[38,39] Its tunable mechanical properties can reproduce the *in vivo* micro-environment stiffness and its porosity enables the free diffusion of salt and small molecules like proteins[40] (pore size <30 nm in 2% agarose). Indeed, medium exchange in the microfluidic chamber is governed by two main mechanisms: (1) flow convection above the hydrogel, (2) diffusion of ions and molecules within the hydrogel (no convective flow within the hydrogel). Thus, the hydrogel acts as a scaffold for spheroid growth and prevents from any shear stress.

Electrical characterization of the microsystem

In order to determine the electric field effectively perceived by the spheroids inside the microfluidic chamber, the device was fully characterized. This characterization process is not

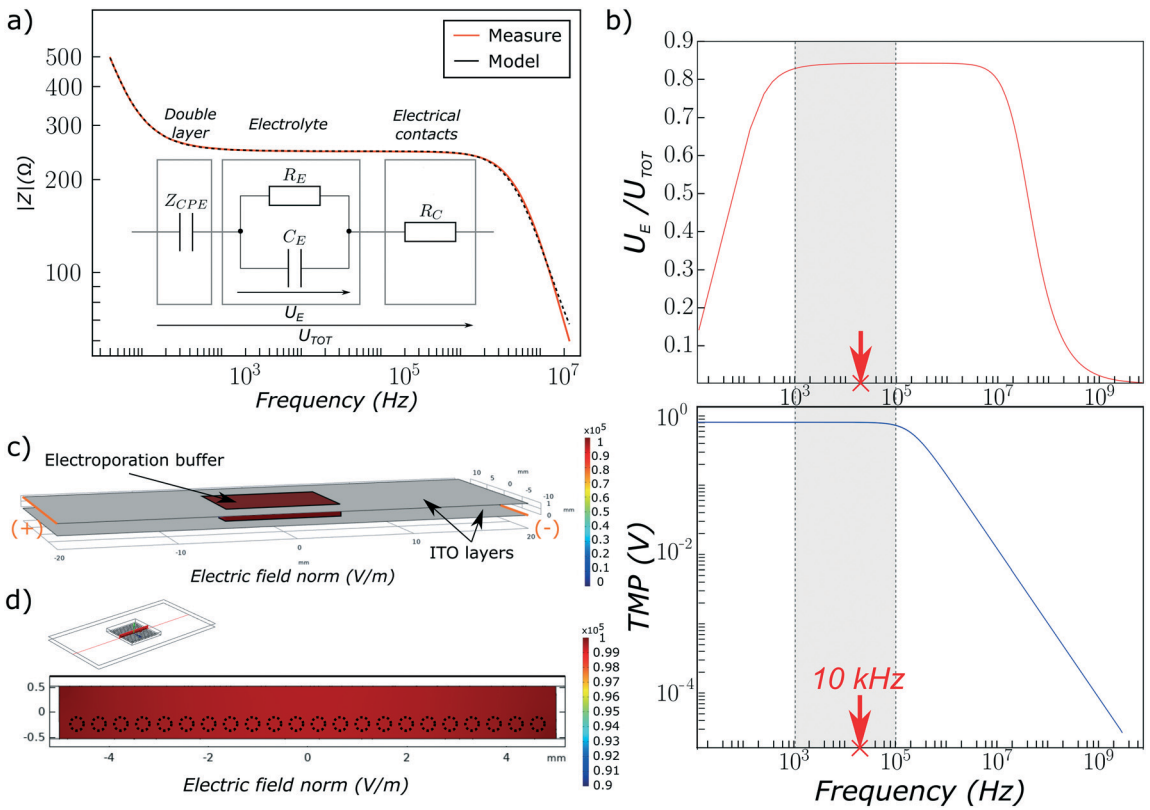

Fig. 2 Characterization of the electric field perceived by spheroids. (a) Impedance module measurement (red solid line), fitting model (black dotted line), and equivalent electrical circuit diagram of the device, with R_E = 245 Ω, C_E = 1.07 × 10^{-10} F, R_C = 43 Ω. (b) Electrical potential in the chamber (U_e) compared to the one applied (U_{tot}) in the device (red line) and characterization of the evolution of transmembrane potential (TMP) of HT29 cells (blue line) with frequency (detailed explanations are presented in Fig. SI 3†). (c) COMSOL model of the microfluidic chamber and electric field distribution. (d) Simulated electric field norm on a cross-section of the chamber containing the spheroids. Dotted circles = spheroids (not included in the model).

always done for other microsystems using ITO electrodes[26,41] even though it is especially important because of the lower electrical conductivity of ITO compared to other metals, which can lead to significant voltage drop, depending on the design. Although electric field distribution in the EPN microfluidic devices is sometimes determined with multiphysics modeling,[27,29,42] the approach used here also includes experimental determination of voltage drop due to contacts and ITO electrode thanks to impedance measurements.

Fig. 2a shows the modeled impedance amplitude (dotted line) fitted to experimental measurements (red line) in the microsystem containing hydrogel and EPN buffer without spheroids. This model takes into account the electrolyte inside the microfluidic chamber, which can be represented by a RC parallel circuit,[43] electrical contacts and wires corresponding to a resistance in series to this circuit, and the interface between electrode and electrolyte. This interface corresponds to an electrical double layer of ions, whose behavior depends on the frequency. It can be modelled by a constant phase element (CPE) to take into account the double layer imperfect capacitive nature.[44] The impedance Z_{CPE} of this double layer is therefore described by: $Z_{CPE} = K(j\omega)^{-\beta}$, with K the impedance amplitude, ω the pulsation, and β a constant between 0 and 1 (equal to 0.9 here). This constant represents the resistive (close to 0) or capacitive (close to 1) nature of the double layer. The equivalent electrical circuit obtained is represented in Fig. 2a.

This model allowed to extract the electric parameters of the equivalent electrical circuit, and thus to calculate the voltage to the terminals of the microfluidic chamber (electrolyte) U_E compared to the total voltage in the system U_{TOT} (Fig. 2b, red line), as detailed in Fig. SI 3.† At low frequencies ($<10^3$ Hz), the impedance is mainly influenced by the capacitive behavior of the ionic double layer at the interface electrode-electrolyte, whereas at higher frequencies (10^3 to 10^7 Hz), the impedance represents the resistive part of the electrolyte. Frequencies higher than 10^7 Hz are not considered in this study, as EPN is performed well below this frequency (around 10 KHz).

The transmembrane potential (TMP) V induced by this applied field can be estimated thanks to the following expression:[45]

$$V = 1.5ER\cos(\theta)\,\frac{1}{1+j\omega\tau_m},$$

where E is the amplitude of the applied electric field (here 800 V cm^{-1}), θ the angle between electric field direction and the normal to the cell membrane (taken equal to 0), $\omega = 2\pi f$ the pulsation, and τ_m a time constant depending on the electrical properties of cells studied here (HT29 cells) which can be found in the MyDEP software,[14,46] and detailed in Fig. SI 3.†

Fig. 2b (blue line) shows that HT29 cells TMP has first-order lowpass filter behavior. The choice of the working frequency for the applied sine burst is 10 kHz, frequency in the middle of the possible range of frequency minimizing voltage drop and maximizing TMP (gray zone in Fig. 2b). Voltage drop at this frequency is around 15%, as we can see in Fig. 2b that the voltage inside the chamber containing the spheroids is equal to 85% of the applied voltage at 10 kHz.

Concerning the electric field inside the chamber, COMSOL modelling (Fig. 2c) shows a homogeneous distribution. As shown on Fig. 2d, there is less than 1% variation on a cross-section of the chamber (values between 990 and 1000 V cm^{-1}). These results ensure that all spheroids are submitted to the same electric field conditions. The potential applied to the terminals of the electrodes, represented by the two layers, was 106 V_{RMS}, the effective potential corresponding to the highest potential tested, 300 V_{pp}. The effect of the double layer is not considered since it is negligible at the working frequency of 10 kHz (Fig. 2a) but the voltage drop due to the low conductivity of the ITO is well considered as the ITO layers modelled have the thickness, conductivity and permittivity measured on the ITO electrodes used in the experiments. COMSOL module "Heat Transfer in Fluids" was also used to estimate the elevation of temperature due to the application of pulsed electric field during EPN. The estimated elevation of temperature, induced by the application of an electric field of the same amplitude and duration as the one used experimentally, is only 0.2 °C, which will not damage cells.

Medium exchange inside the hydrogel

To ensure reproducible EPN conditions, and in particular the conductivity inside the microfluidic chamber containing spheroids, medium exchange was characterized by injecting EPN buffer in the chamber containing a hydrogel saturated with culture medium. Results presented in Fig. 3 show that medium exchange inside the whole chamber, including the hydrogel, is easy and quick: 2.5 mL injected in 10 minutes.

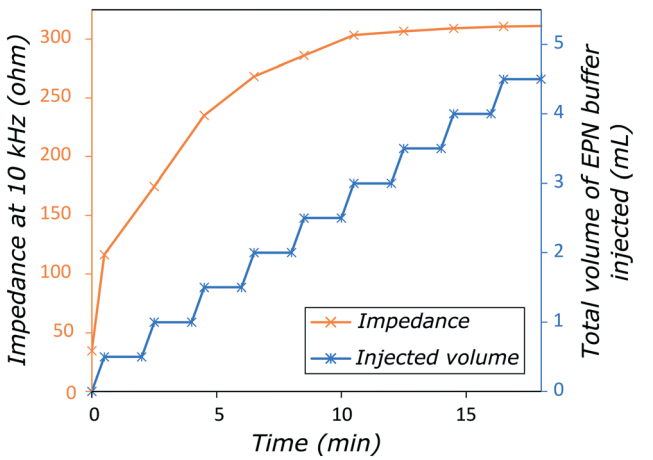

Fig. 3 Study of medium exchange from culture medium to EPN buffer inside the microfluidic chamber by impedance measurement. Orange line = impedance amplitude curve, blue line = volume injected.

Therefore, the microsystem enables a gentle medium exchange with a small flow without complicated manipulation that may damage spheroids. By applying the injection protocol thus determined, conductivity inside the chamber will thus be reproducible for all experiments performed in the microsystem. These results were confirmed by monitoring medium exchange inside the hydrogel, when injecting a fluorescence solution, with confocal microscopy (Fig. SI 4†).

Determination of parameters for efficient EPN in the microsystem

Electric field parameters for efficient EPN in the microsystem were determined by varying the amplitude of the applied sine bursts. The other parameters were fixed. The relevance of such waveform for small molecule delivery into cells has recently been pointed out,[33] as its simple spectral content can help to better understand the EPN phenomenon and its dependance to frequency. Moreover, the application of alternating current signals enables the reduction of electrochemical phenomena that can damage such thin film electrodes.[32] The sine frequency was 10 kHz as explained in the previous section. The duration, number of bursts and repetition frequency of pulses, respectively 5 ms and 2 bursts spaced by 1 s, were chosen based on the literature[33] and kept unchanged for all the experiments. As noted before,[47] these parameters influence the concentration of pores formed at the membrane surface. Pulse duration can also influence the efficiency for larger target molecules, such as DNA plasmid, with the contribution of phenomena such as electrophoresis to help DNA move towards cells.[48] However, in this study, only small molecules are considered, so we only focused on sine burst amplitude to determine the EPN threshold to deliver such molecules into the studied HT29 cells.

EPN was first realized in the microsystem containing grown HT29 spheroids, in presence of two fluorophores: FDA and PI. FDA labels living cells in green and PI is a small fluorescent molecule that can penetrate only in cells temporarily permeabilized by the pulsed electric field applied.[29,36] Thus, when cells were electroporated in presence of PI and FDA, those displaying both green and red fluorescence could be considered as alive and electroporated. Therefore, merged fluorescent signals showing yellow intersections can be related to reversible and efficient EPN. Fluorescence was observed 5 min after EPN for amplitudes of 100 to 200 V_{pp}, with an epifluorescence microscope.

The correspondence between the amplitude peak-to-peak A_{pp} of the applied sine burst and the effective electric field E_{RMS} is given by:

$$E_{RMS} = \frac{0.85 \times A_{pp}}{2\sqrt{2}d},$$

with d = 1 mm the distance between electrodes. The factor 0.85 is used to consider the voltage drop of 15% due to electrical contacts and ITO thin layer, estimated thanks to

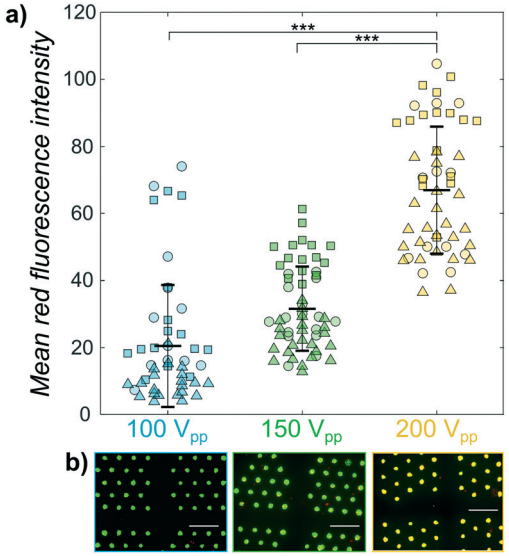

Fig. 4 Determination of EPN threshold with epifluorescence microscopy. (a) Mean red fluorescence intensity of each spheroid on maximum intensity projection (MIP) epifluorescence images (10×) realized on HT29 cell spheroids 5 min after EPN in presence of FDA and PI. Blue = 100 V_{pp}, green = 150 V_{pp}, yellow = 200 V_{pp}, point/square/triangle = value for one spheroid imaged, long horizontal line = mean, small horizontal line = STD value, N = [12 to 24] spheroids/experiment, ***$p < 0{,}001$, triplicate (points, squares and triangles correspond to results from 3 different experiments). (b) MIP merged epifluorescence images (2.5×) of these spheroids. Green = FDA, red = PI, yellow = both, scale bar = 1 mm.

Fig. 2b. Therefore, the amplitudes tested, namely 100 to 300 V_{pp}, correspond to effective electric fields perceived by spheroids of 300 to 900 V_{RMS} cm^{-1}. It should be noted that electrical losses are not often considered in the literature, and the electric field values given are usually those applied, rather than those effectively perceived by spheroids. Hence, comparison between the different studies is complicated, because electrical losses may not be of the same order of magnitude for all microsystems or EPN devices used.

The results presented in Fig. 4a enable to determine a first EPN threshold of 200 V_{pp} for our experiment, as fluorescence intensity is of similar and significantly lower level for 100 and 150 V_{pp}. It can also be qualitatively visualized in Fig. 4b, on which the spheroids appear in yellow (*i.e.* merged fluorescence signals of both alive and electroporated cells) only for 200 V_{pp} applied. The microscopic images, taken at the minimum magnification and representing only an eight of the whole chamber, illustrate the fact that the microsystem developed here enables the observation of tens of spheroids simultaneously. Indeed, it was possible to perform EPN at once on a large number of spheroids with no handling steps. Thus, it reduced the time of an EPN experiment compared to other existing devices used in the litterature,[15,23] where spheroids are often cultivated in multi-well plates, requiring to repeat each step for each spheroid treated. Unlike in these multi-well plates, here medium exchange steps and EPN procedure do not disturb spheroids thanks to the micro-

structured hydrogel and the microfluidic system. Moreover, the microsystem enabled *in situ* imaging with a simple optical technique, epifluorescence, which allowed to calibrate EPN parameters quickly and easily.

To assess the mortality due to the EPN conditions applied, a viability assay was realized on electroporated spheroids. The same fluorophore, PI, was used for both EPN efficiency and cell viability assays, as often reported in the literature.[26,29,36] Indeed, PI is a marker of membrane integrity loss, characteristic of dead cells. A comparison of red fluorescence intensity measured on dead spheroids and electroporated spheroids was realized to illustrate this double use of PI, showing a significantly higher intensity for dead spheroids (Fig. SI 5†). Therefore, a live/dead labelling using FDA and PI was made on spheroids 2 h after EPN. Results (Fig. SI 6†) demonstrate a very low mortality (less than 3%) due to the pulsed electric field applied, ensuring that the EPN conditions determined are reversible.

To evaluate EPN efficiency for higher amplitudes (250 and 300 V_{pp}), another experiment was realized with confocal microscopy, which enabled to visualize the inner part of the spheroid and therefore to assess EPN efficiency in the core of the spheroids. To do that, we observed fixed spheroids with confocal microscopy at 25× magnification (Fig. 5a). We computed the evolution of the mean intensity of PI fluorescence confocal images depending on the distance from the spheroid periphery to the core (Fig. 5b), to determine the level of electroporation of cells inside spheroids, for several electric field intensities applied. Results are normalized for each spheroid compared to the spheroid diameter, to obtain the distance ratio r from the periphery (r = 0) to the core (r = 1) of each spheroid. This intensity is also normalized compared to the intensity of the periphery (r = 0) for 300 V_{pp} applied, as it corresponds to the higher electric field applied. A dead control (data not shown) demonstrated that the clarification technique used, adding glycerol on the spheroids, is efficient to allow the observation inside these spheroids of 116 ± 23 μm diameter, as there is nearly no diminution of fluorescence intensity due to photon absorption.

Results show that EPN is more efficient for the highest amplitude of sine burst applied, namely 300 V_{pp} (corresponding to 900 V_{RMS} cm^{-1}). For 250 V_{pp} (750 V_{RMS} cm^{-1}) and 200 V_{pp} (600 V_{RMS} cm^{-1}), EPN is respectively 25% and 45% less efficient. Concerning the EPN efficiency inside spheroids, there is a decrease of 25 to 30% from the periphery to the core for 250 and 300 V_{pp}, and more than 40% for 200 V_{pp}. For the two highest amplitudes applied, the intensity in the core stays above 50% of the maximum intensity measured, showing a good EPN efficiency for the entire spheroid volume. However, for 200 V_{pp}, cells located in the core of the spheroids are less electroporated, as the intensity level decreases to a value close to the one obtained for 150 V_{pp} applied, for which only few cells are permeabilized. This could be due to a decrease in cell size in the core of the spheroids[49] and therefore a decrease in cell sensitivity to the electric field applied, as the induced transmembrane potential is linearly dependent on the cell radius.[50]

Concerning voltages below the determined threshold, namely 100 and 150 V_{pp}, results are consistent with the ones obtained from epifluorescence microscopy (Fig. 4), as the

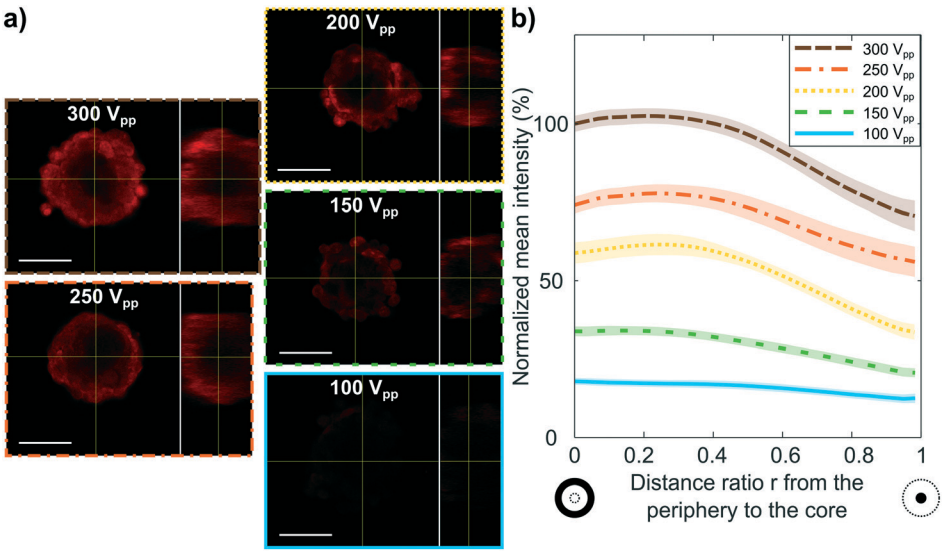

Fig. 5 Study of EPN efficiency inside spheroids for several amplitudes of applied voltage thanks to confocal microscopy. (a) Typical confocal microscope z-stack images (25×) for a slice in the core of HT29 cell spheroids and corresponding orthogonal view. Red = PI, scale bar = 100 μm. Electroporated cells incorporate PI and appear red. (b) Mean intensity of fixed spheroids electroporated with PI (red) as a function of the distance from the periphery to the core of the spheroid (116 ± 23 μm diameter), normalized by the mean intensity at the periphery (r = 0) of spheroids electroporated at 300 V_{pp}, and by the maximum radius of each spheroid. Brown = 300 V_{pp}, orange = 250 V_{pp}, yellow = 200 V_{pp}, green = 150 V_{pp}, blue = 100 V_{pp}, shaded area = SEM values, N = 20 spheroids/condition, duplicate.

mean intensity measured is 60 to 75% less than the one measured for an EPN voltage of 300 V_{pp}. It can be noted that the difference between periphery and core intensities for 100 and 150 V_{pp} is less visible than for 200 V_{pp}, but it is due to the fact that the intensity measured for these low voltages is so small (close to noise level) that it is not possible to determine if cells in the core of the spheroids are less electroporated than those at the periphery, especially for the lowest applied electric field.

This study highlights the potential of the device to characterize EPN efficiency in the core of tens of spheroids in a single experiment. Such analysis is not often conducted on spheroids and could be very useful to better understand the effect of pulsed electric field on 3D constructs, or to characterize the effect of EPN-based treatments inside spheroids. As noted in the few previous studies available in the litterature,[11,36] results show that permeabilization is efficient from the periphery to the core of spheroids, with a small decrease in the core of the spheroid. Concerning the EPN parameters, 300 V_{pp} will be chosen as the applied voltage for the application of the device to ECT, as it seems to be more efficient than the other voltages tested. This value corresponds to an effective field of 900 V_{RMS} cm^{-1}, or 1030 V_{RMS} cm^{-1} if voltage drop is not considered which is close to the one used for similar studies of EPN efficiency on spheroids.[23,51–53]

Application to electro-chemotherapy: EPN of drug in cancer cell spheroids

After the demonstration of the microsystem ability to perform reversible EPN on spheroids, a first application as

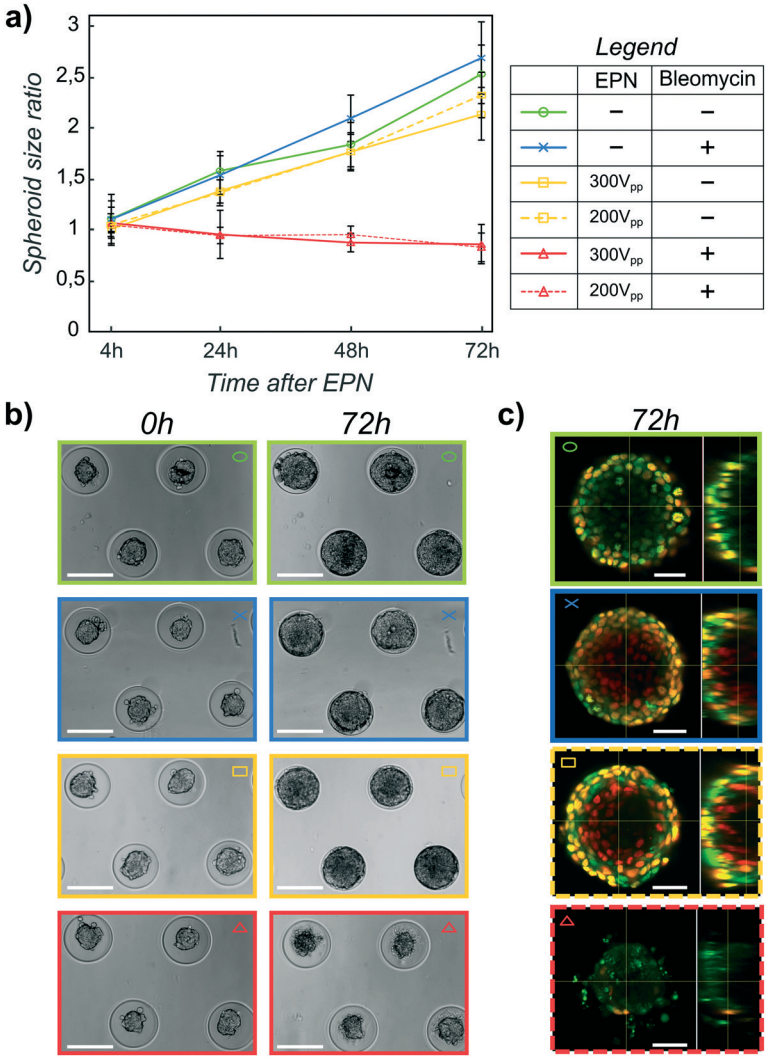

Fig. 6 Study of the effect of ECT treatment with bleomycin on HT29 cell spheroid growth and cell proliferation. (a) HT29 cell spheroid surface ratio evolution after experiment with (+) and/or without (–) EPN and/or bleomycin for several conditions: green = non-treated spheroids, blue = bleomycin only, yellow = EPN only, red = EPN with bleomycin, solid line = 300 V_{pp}, dotted line = 200 V_{pp}, N = [10 to 15] spheroids/experiment, triplicate. (b) Optical microscope images (4×) of spheroids before and 72 h after the experiment. Scale bar = 200 μm. (c) Orthogonal views of confocal microscope images of spheroids 72 h after this experiment, representing cell nuclei in green and proliferative cells in red. Green = NucGreen, red = EdU, yellow = both, scale bar = 50 μm.

in vitro drug testing platform was realized. The same EPN procedure was used, except for the addition of an anticancer drug in the EPN buffer instead of fluorophores. A commonly used anticancer drug, bleomycin, was chosen to study the electro-chemotherapy (ECT) effect on HT29 cell spheroids, for sake of comparison with similar previous study.[53] It has the particularity to enter only in cells that are permeabilized, and to intercalate in DNA to stop cell division. The EPN voltage applied for the experiments presented in Fig. 6 was 200 V_{pp} or 300 V_{pp}, to compare a higher voltage that induces more efficient permeabilization with a lower voltage, inducing less cell mortality (Fig. SI 6†). Growth monitoring after this experiment (Fig. 6a and b) demonstrates that spheroids submitted to electroporation only, or to bleomycin without EPN, show the same growth rate as to the control spheroids without EPN and bleomycin. On the contrary, spheroids treated with EPN in presence of bleomycin, display growth inhibition, as it can be seen in red on the graph and on the corresponding microscope images (Fig. 6b).

Thanks to the micro-structured hydrogel encompassing the spheroids, it was possible to perform a proliferation labeling of all spheroids at once, with a commercial kit revealing EdU incorporation in cells. Therefore, it considerably reduced the duration of the experiment, preventing to repeat all steps of the protocol for each well containing one spheroid, as it is the case for ultra-low adhesion plates. All nuclei were also stained, with the NucGreen marker, to be able to see all cells by fluorescence confocal microscopy, and not only the proliferative ones. The EPN voltage for this experiment was of 200 V_{pp}, as the effect on growth is similar to the one at 300 V_{pp}, and observations were made three days after the experiment. It shows that cell proliferation, appearing in yellow because of the superposition of nucleus (green) and EdU labeling (red), was similar for all control groups (*i.e.* non-treated spheroids, bleomycin only and EPN only). A few layers of proliferative cells can be seen on the orthogonal views realized on ImageJ (Fig. 6c). However, for spheroids treated with electro-chemotherapy (*i.e.* EPN in presence of bleomycin), there are nearly no proliferative cells and cell nuclei seem to be exploded. The proliferative layer was further quantified from *z*-stack confocal images and estimated to be between 1 to 3 cell layers for all control groups, while no proliferative layer remains for the ECT/bleomycin-treated spheroids (Fig. SI 7†).

These results are consistent with the non-permeant character of cells to bleomycin and its efficacy only on permeabilized cells. It is one of the reasons why this molecule is particularly advantageous for ECT applications, because it helps reducing side effects of chemotherapy,[54,55] as it is not harmful for non-electroporated healthy cells around the tumor, that can be in contact with bleomycin during its injection in the tumor tissues. Results of Fig. 6 also confirm the reversibility of the electroporation conditions used here, as electroporation has no impact on spheroid growth and proliferation. Even though the two voltages applied seem to have a different effect on cell viability (Fig. SI 6†), they induce a similar growth evolution, comparable to the one of healthy spheroids. These results are consistent with the litterature,[36,53] showing a growth inhibition effect of the anticancer drug for ECT/bleomycin treated spheroids only.

It can also be noted that ECT/bleomycin has the same effect on growth for the two EPN voltages tested, although it has been shown that 300 V_{pp} EPN was more efficient (Fig. 5). This shows that even if a small quantity of bleomycin penetrates in cells, it may be sufficient to stop their division. Interestingly, various concentrations of bleomycin are tested in the literature, from 1 mM,[36] close to concentrations used *in vivo*, to 10 μM,[22] 100 times less. Even if we used a 14 μM bleomycin during our experiments, we noticed that a lower concentration of bleomycin could also inhibit spheroid growth three days after EPN (data not shown), as it was demonstrated elsewhere.[56] Therefore, bleomycin concentrations used *in vitro* reported in the literature might be sometimes overdosed.

Conclusion

The research work presented here shows that the developed microsystem enables culture, monitoring, and electroporation (EPN) of a large number of spheroids in a unique system, and demonstrates its application as a lab-on-a-chip anticancer drug testing platform. Indeed, the micro-structured hydrogel[30] integrated into the microfluidic chamber allows the production of more than 300 spheroids of similar size, shape, and of known and reproducible location, an important asset to get statistically relevant and reproducible results. These spheroids better mimic complex tumor tissues than 2D cell culture or cells in suspension,[10] enabling relevant test of treatments based on EPN, such as electro-chemotherapy (ECT), that can improve cancer treatments.[4]

The microsystem was fully characterized, with impedance measurements and modeling, showing a homogeneous distribution of the electric field. It ensures that all spheroids are submitted to the same EPN conditions. These parameters could be easily determined thanks to *in situ* observation, with several techniques from simple optical microscopy to more complex epifluorescence and confocal microscopy, enabling EPN efficiency evaluation even in the core of the spheroids. To increase the throughput, the microsystem can be mounted between standard cover-slip and glass slides, after having fixed the spheroids, making it fully compatible with automatic high content screening platform.[57] We also intend to use electrodes to perform bio-impedance measurements in order to study EPN effect[58] or monitor spheroid growth.

The integrated device presented here is also compatible with more complex spheroid models, as well as organoids. To get closer to *in vivo* tumor tissues, future work will focus on complexifying the multicellular spheroids models to analyze the effect of various parameters on EPN efficiency such as spheroid size[18] and tumor microenvironment,[59,60] including

cancer-associated cells[61] and the extracellular matrix. These complexified models will be used to test other ECT molecules like calcium, which has been identified as a promising treatment with a reduced effect on healthy cells compared to malignant ones.[53] Future studies will also aim at adapting the microsystem for electro-gene therapy (EGT) application. This will pave the way for CRISPR/Cas9 transfection on organoids derived from patients,[62,63] therefore increasing even more the potential applications of the device for both fundamental research and precision medicine.[64]

Conflicts of interest

There are no conflicts of interest to declare.

Acknowledgements

This work was supported by the LABEX iMUST (ANR-10-LABX-0064) of Université de Lyon, within the program "Investissements d'Avenir" (ANR-11-IDEX-0007) operated by the French National Research Agency (ANR). It was also financially supported by the CNRS MITI (Troposphere project), by the "Institut Universitaire de France" (IUF) and by the Région Auvergne-Rhône-Alpes (E-3D cell). The authors would like to acknowledge Radoslaw Mazurczyk and Claude Botella from NanoLyon technological platform for their support with the characterization of the ITO conductive layer; Pascal Bevillacqua for his work on the first prototype of the microsystem; Martin Guillemaud, Victor Perrin and Théo Le Berre for their investment on this project during their internship; as well as Sylvain Monnier and Gilles Simon for the design and fabrication of the micro-milled master mold.

References

1 L. M. Mir, M. Belehradek, C. Domenge, S. Orlowski, B. Poddevin, J. J. Belehradek, G. Schwaab, B. Luboinski and C. Paoletti, *C. R. Acad. Sci., Ser. III*, 1991, **313**, 613–618.
2 E. Neumann and K. Rosenheck, *J. Membr. Biol.*, 1972, **10**, 279–290.
3 K. Kinosita and T. Y. Tsong, *Nature*, 1977, **268**, 438–441.
4 I. Edhemovic, E. M. Gadzijev, E. Brecelj, D. Miklavcic, B. Kos, A. Zupanic, B. Mali, T. Jarm, D. Pavliha, M. Marcan, G. Gasljevic, V. Gorjup, M. Music, T. P. Vavpotic, M. Cemazar, M. Snoj and G. Sersa, *Technol. Cancer Res. Treat.*, 2011, **10**, 475–485.
5 C. Y. Calvet and L. M. Mir, *Cancer Metastasis Rev.*, 2016, **35**, 165–177.
6 Veterinary electrochemotherapy treat cutaneous tumors, **https://www.leroybiotech.com/electrochemotherapy/electrochemotherapy-in-veterinary-medicine/**, (accessed 7 October 2021).
7 L. Pasquet, E. Bellard, S. Chabot, B. Markelc, M.-P. Rols, J. Teissie and M. Golzio, *J. Immunother. Cancer*, 2019, **7**, 161.
8 M. Pavlin, M. Kandušer, M. Reberšek, G. Pucihar, F. X. Hart, R. Magjarevićcacute and D. Miklavčič, *Biophys. J.*, 2005, **88**, 4378–4390.
9 A. G. Pakhomov, D. Miklavcic and M. S. Markov, *Advanced Electroporation Techniques in Biology and Medicine*, CRC Press, 2010.
10 J. Hoarau-Véchot, A. Rafii, C. Touboul and J. Pasquier, *Int. J. Mol. Sci.*, 2018, **19**, 181.
11 L. Wasungu, J.-M. Escoffre, A. Valette, J. Teissie and M.-P. Rols, *Int. J. Pharm.*, 2009, **379**, 278–284.
12 M. Zanoni, F. Piccinini, C. Arienti, A. Zamagni, S. Santi, R. Polico, A. Bevilacqua and A. Tesei, *Sci. Rep.*, 2016, **6**, 19103.
13 W. Liao, J. Wang, J. Xu, F. You, M. Pan, X. Xu, J. Weng, X. Han, S. Li, Y. Li, K. Liang, Q. Peng and Y. Gao, *J. Tissue Eng.*, 2019, **10**, 1–15.
14 J. M. Huber, A. Amann, S. Koeck, E. Lorenz, J. M. Kelm, P. Obexer, H. Zwierzina and G. Gamerith, *J. Cancer Res. Clin. Oncol.*, 2016, **142**, 1955–1966.
15 M. Fiorentzis, A. Viestenz, B. Seitz, S. E. Coupland and J. Heinzelmann, *J. Visualized Exp.*, 2020, 60611.
16 I. W. Mak, N. Evaniew and M. Ghert, *Am. J. Transl. Res.*, 2014, **6**, 114–118.
17 Y.-C. Tung, A. Y. Hsiao, S. G. Allen, Y. Torisawa, M. Ho and S. Takayama, *Analyst*, 2011, **136**, 473–478.
18 L. Gibot and M.-P. Rols, *J. Membr. Biol.*, 2013, **246**, 745–750.
19 Y. Tang, J. Liu and Y. Chen, *Microelectron. Eng.*, 2016, 5.
20 G. Fang, H. Lu, A. Law, D. Gallego-Ortega, D. Jin and G. Lin, *Lab Chip*, 2019, 12.
21 G. Covello, K. Siva, V. Adami and M. A. Denti, *Cytotechnology*, 2014, **66**, 543–553.
22 S. K. Frandsen, H. Gissel, P. Hojman, J. Eriksen and J. Gehl, *Biochim. Biophys. Acta, Gen. Subj.*, 2014, **1840**, 1204–1208.
23 L. Gibot, A. Montigny, H. Baaziz, I. Fourquaux, M. Audebert and M.-P. Rols, *Cancers*, 2020, **12**, 425.
24 M. B. Fox, D. C. Esveld, A. Valero, R. Luttge, H. C. Mastwijk, P. V. Bartels, A. van den Berg and R. M. Boom, *Anal. Bioanal. Chem.*, 2006, **385**, 474–485.
25 S. Movahed and D. Li, *Microfluid. Nanofluid.*, 2011, **10**, 703–734.
26 Y. Xu, H. Yao, L. Wang, W. Xing and J. Cheng, *Lab Chip*, 2011, **11**, 2417.
27 S. Bian, Y. Zhou, Y. Hu, J. Cheng, X. Chen, Y. Xu and P. Liu, *Sci. Rep.*, 2017, **7**, 42512.
28 G.-B. Lee, C.-J. Chang, C.-H. Wang, M.-Y. Lu and Y.-Y. Luo, *Microsyst. Nanoeng.*, 2015, **1**, 15007.
29 Q. Zhu, M. Hamilton, B. Vasquez and M. He, *Lab Chip*, 2019, **19**, 2362–2372.
30 C. Rivière, A. Prunet, L. Fuoco and H. Delanoë-Ayari, Patent FR3079524A1, 2018, **https://patents.google.com/patent/FR3079524B1/en**.
31 S. Goodarzi, A. Prunet, F. Rossetti, G. Bort, O. Tillement, E. Porcel, S. Lacombe, T.-D. Wu, J.-L. Guerquin-Kern, H. Delanoë-Ayari, F. Lux and C. Rivière, *Lab Chip*, 2021, **21**, 2495–2510.
32 S. Mahnič-Kalamiza and D. Miklavčič, *Electrochim. Acta*, 2020, **363**, 137187.
33 T. García-Sánchez, C. Merla, J. Fontaine, A. Muscat and L. M. Mir, *Biochim. Biophys. Acta, Biomembr.*, 2018, **1860**, 1022–1034.

34 P. Bregigeon, J. Marchalot, L. Franqueville, C. Vollaire, M. Frénéa-Robin and C. Rivière, in *The 25 th International Conference on Miniaturized Systems for Chemistry and Life Sciences (MicroTAS2021)*, Palm Springs and Online, 2021.
35 A. Ahmad, S. Goodarzi, C. Frindel, G. Recher, C. Riviere and D. Rousseau, BioRxiv, 2021, DOI: **10.1101/2021.01.31.428996**.
36 L. Gibot, L. Wasungu, J. Teissié and M.-P. Rols, *J. Controlled Release*, 2013, **167**, 138–147.
37 A. Desmaison, C. Frongia, K. Grenier, B. Ducommun and V. Lobjois, *PLoS One*, 2013, **8**, e80447.
38 J. Rosser, I. O. Calvo, M. Schlager, M. Purtscher and P. Ertl, *J. Cell Biol. Cell Metab.*, 2015, **2**, 15.
39 P. Zarrintaj, S. Manouchehri, Z. Ahmadi, M. R. Saeb, A. M. Urbanska, D. L. Kaplan and M. Mozafari, *Carbohydr. Polym.*, 2018, **187**, 66–84.
40 A. Pluen, P. A. Netti, R. K. Jain and D. A. Berk, *Biophys. J.*, 1999, **77**, 542–552.
41 S.-C. Chen, T. S. Santra, C.-J. Chang, T.-J. Chen, P.-C. Wang and F.-G. Tseng, *Biomed. Microdevices*, 2012, **14**, 811–817.
42 T. Jain, A. Papas, A. Jadhav, R. McBride and E. Saez, *Lab Chip*, 2012, **12**, 939.
43 N. G. Green, A. Ramos, A. González, H. Morgan and A. Castellanos, *Phys. Rev. E: Stat., Nonlinear, Soft Matter Phys.*, 2002, **66**, 026305.
44 E. T. McAdams, A. Lackermeier, J. A. McLaughlin, D. Macken and J. Jossinet, *Biosens. Bioelectron.*, 1995, **10**, 67–74.
45 T. Kotnik and D. Miklavcic, *IEEE Trans. Biomed. Eng.*, 2000, **47**, 1074–1081.
46 J. Cottet, O. Fabregue, C. Berger, F. Buret, P. Renaud and M. Frénéa-Robin, MyDEP: a new computational tool for dielectric modeling of particles and cells, *Zenodo*, 2019.
47 M.-P. Rols and J. Teissié, *Biophys. J.*, 1998, **75**, 1415–1423.
48 M. Golzio, J. Teissie and M.-P. Rols, *Proc. Natl. Acad. Sci. U. S. A.*, 2002, **99**, 1292–1297.
49 Y. L. Han, A. F. Pegoraro, H. Li, K. Li, Y. Yuan, G. Xu, Z. Gu, J. Sun, Y. Hao, S. K. Gupta, Y. Li, W. Tang, X. Tang, L. Teng, J. J. Fredberg and M. Guo, *Nat. Phys.*, 2020, **16**, 101–108.
50 H. P. Schwan, in *Advances in Biological and Medical Physics*, Elsevier, 1957, vol. 5, pp. 147–209.
51 M. Fiorentzis, A. Viestenz, U. Siebolts, B. Seitz, S. E. Coupland and J. Heinzelmann, *Cancers*, 2019, **11**, 1344.
52 Y.-S. Choi, H.-B. Kim, G.-S. Kwon and J.-K. Park, *Biomed. Microdevices*, 2009, **11**, 151–159.
53 S. K. Frandsen, L. Gibot, M. Madi, J. Gehl and M.-P. Rols, *PLoS One*, 2015, **10**, e0144028.
54 D. C. Bloom and P. M. Goldfarb, *Eur. J. Surg. Oncol.*, 2005, **31**, 1029–1035.
55 B. Geboers, H. J. Scheffer, P. M. Graybill, A. H. Ruarus, S. Nieuwenhuizen, R. S. Puijk, P. M. van den Tol, R. V. Davalos, B. Rubinsky, T. D. de Gruijl, D. Miklavčič and M. R. Meijerink, *Radiology*, 2020, **295**, 254–272.
56 M. J. Jaroszeski, V. Dang, C. Pottinger, J. Hickey, R. Gilbert and R. Heller, *Anti-Cancer Drugs*, 2000, **11**, 201–208.
57 O. Sirenko, T. Mitlo, J. Hesley, S. Luke, W. Owens and E. F. Cromwell, *Assay Drug Dev. Technol.*, 2015, **13**, 402–414.
58 T. García-Sánchez, M. Guitart, J. Rosell-Ferrer, A. M. Gómez-Foix and R. Bragós, *Biomed. Microdevices*, 2014, 16.
59 G. Lazzari, V. Nicolas, M. Matsusaki, M. Akashi, P. Couvreur and S. Mura, *Acta Biomater.*, 2018, **78**, 296–307.
60 X. Xin, H. Yang, F. Zhang and S.-T. Yang, *Process Biochem.*, 2019, **78**, 148–160.
61 M. Zoetemelk, M. Rausch, D. J. Colin, O. Dormond and P. Nowak-Sliwinska, *Sci. Rep.*, 2019, **9**, 7103.
62 D. Tuveson and H. Clevers, *Science*, 2019, **364**, 952–955.
63 A. K. Fajrial, Q. Q. He, N. I. Wirusanti, J. E. Slansky and X. Ding, *Theranostics*, 2020, **10**, 5532–5549.
64 R. W. Peck, C. D. Hinojosa and G. A. Hamilton, *Clin. Pharmacol. Ther.*, 2020, **107**, 181–185.